Synthesis of a Series of Zinc Porphyrins and Spectroscopic Changes upon Coordination Reaction with Imidazole Derivatives

Shu-Jun Wang,* Yu-Ling Peng, Cheng-Gen Zhang, Yong-Bing Li, and Chao Liu

*College of Chemistry and Materials Science, Langfang Teachers University, Langfang 065000, People's Republic of China. *E-mail: d022036@mail.nankai.edu.cn*
Received June 16, 2015, Accepted July 26, 2015, Published online October 4, 2015

Three metal-free porphyrins modified with Boc-L-threonine and their zinc analogs were synthesized and characterized by elemental analysis, ^{1}H NMR, UV/vis, and fluorescence spectroscopies. The binding of imidazole derivatives to these zinc porphyrins was studied, with emphasis on the binding mechanism in CH_2Cl_2 solution, by means of UV/vis spectroscopy and quantum chemical methods. Both experimental results and theoretical calculations showed that a coordination reaction occurred between the zinc porphyrins and imidazole derivatives. The association constants between the zinc porphyrins and imidazole derivatives decreased in the order *N*-MeIm>Im. Increasing the temperature disfavored the interaction. Thermodynamic parameters calculated by the van't Hoff equation showed that the driving force for the reaction was the enthalpy change. The fluorescence changes associated with the interaction between the zinc porphyrins and imidazole derivatives were also studied by fluorescence spectroscopy. The experimental results showed significant quenching between the various zinc porphyrins and imidazole derivatives.

Keywords: Zinc porphyrins, Coordination reaction, Thermodynamic parameters, Fluorescence quenching, Theoretical calculation

Introduction

Porphyrins are often used as model compounds for some important biological systems due to their unique roles in biology and sensing systems, such as in imitating plants and the reaction center of bacterial photosynthesis, or the active center of cell pigment P-450.[1−14] The axial coordination reaction between a porphyrin and a small molecule containing a nitrogen atom has been widely used as a reaction model of hemoglobin, myoglobin, cytochrome-*c*, and other biological molecules. Upon such axial coordination, the conjugated structure of the porphyrin molecule, characterized by alternating single and double bonds, greatly facilitates electron transfer while also imparting good thermal stability and photoelectric properties.[15−20] Imidazole derivatives with structures similar to that of the natural enzyme ligand are commonly used small molecules in axial coordination reactions. The activation of metal porphyrins by coordination of imidazole derivatives not only enhances their reactivity but also creates the space and structural conditions for reaction. Thus, imidazole derivatives play an important role in oxidation processes, transferring an electron and enhancing the stability of the whole system.[21,22]

The structures and functions of porphyrins modified with amino acids are similar to those of natural porphyrins. Threonine is a common amino acid and has many biological functions. A protein kinase incorporating threonine and showing antiviral activity has been studied by Venditto[23] and Darbinian[24]; this amino acid may provide a new route for developing novel drugs.

In this study, we have used Boc-L-threonine to synthesize three kinds of free porphyrins and their zinc analogs with a view to combining the biological activities of porphyrin and threonine. The coordination reaction between zinc porphyrins and imidazole derivatives has been studied by means of UV/vis spectroscopy and quantum chemical methods. Association constants have been determined at four different temperatures; the binding mechanism in CH_2Cl_2 has been determined; and the fundamental driving force for the coordination system has been elucidated. The quenching properties have been studied by fluorescence spectroscopy. These experimental results may be of value in a variety of areas, such as drug design, protein engineering, and gene technology.

Experimental

Materials and Methods. Pyrrole was distilled, and *p*-nitrobenzaldehyde and imidazole (Im) were recrystallized prior to use. Boc-L-threonine was purchased from Beijing J&K Technology Co., Ltd. (Beijing, China), and was biochemical reagent grade. Dry CH_2Cl_2 was obtained by redistillation from $CaCl_2$. *N*-methylimidazole (*N*-MeIm) and other reagents were commercial chemicals of analytical grade and were used as received without further purification.

Elemental analysis (C, H, N) was performed with a CE-440 elemental analyzer (Exeter Analytical, Inc., North Chelmsford, MA, USA). ^{1}H NMR spectra were recorded at room temperature on a Varian 400 MHz spectrometer (Varian, Inc., Palo Alto, CA, USA) from samples in $CDCl_3$ solution. UV/vis absorption spectra were measured on a Shimadzu 2550

spectrophotometer (Shimadzu Corporation, Kyoto, Japan) equipped with an HH-501 temperature controller in the region 375−750 nm using CH_2Cl_2 as solvent. Fluorescence measurements were made on a Shimadzu F-4600 fluorescence spectrometer (Shimadzu Corporation, Kyoto, Japan) at room temperature.

The Soret and Q bands in the UV/vis spectra of the free porphyrins and zinc porphyrins were measured using 2.5 and 25 μM solutions, respectively. Solutions of Im and *N*-MeIm were added to 2.5 μM solutions of the three respective zinc porphyrins in CH_2Cl_2, and the absorption changes at the Soret band were monitored at four different temperatures. The value *n* of the coordination reactions, the association constants K^{θ}, the enthalpy change $\Delta_r H_m^{\theta}$, and the entropy change $\Delta_r S_m^{\theta}$ were calculated by means of Origin software (OriginLab Corporation, Northampton, MA, USA). Similarly, solutions of Im and *N*-MeIm were added to 2.5 μM solutions of the three respective zinc porphyrins in CH_2Cl_2 at room temperature. The excitation band width and emission band width were both set at 10 nm. The excitation wavelength was 420 nm. The scanning range was 450−750 nm.

All structures were optimized at the B3LYP/BS level. BS denotes a basis set combining LANL2DZ for Zn and 6-31 + G(d) for nonmetal atoms. Harmonic frequency analysis calculations were performed to characterize the optimized structures as true minima (no imaginary frequency). All standard DFT calculations were carried out using the Gaussian 09 program.[25−27]

Synthesis. The synthetic route to the final complex is outlined in Scheme 1. The structures of the imidazole derivatives are shown in Scheme 2.

Porphyrin 1a: A mixture of 4-nitrobenzaldehyde (2.57 g, 0.017 mol), benzaldehyde (5.41 g, 0.051 mol), and pyrrole (0.536 g, 8 mmol) in CH_3CH_2COOH (120 mL) was stirred and heated to reflux for 5 min. After the addition of further pyrrole (4.29 g, 0.064 mol) in CH_3CH_2COOH (25 mL), the reaction mixture was stirred for a further 20 min. The initially colorless solution turned brown. The mixture was allowed

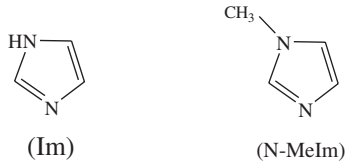

(Im) (N-MeIm)

Scheme 2. Structure of imidazole derivatives.

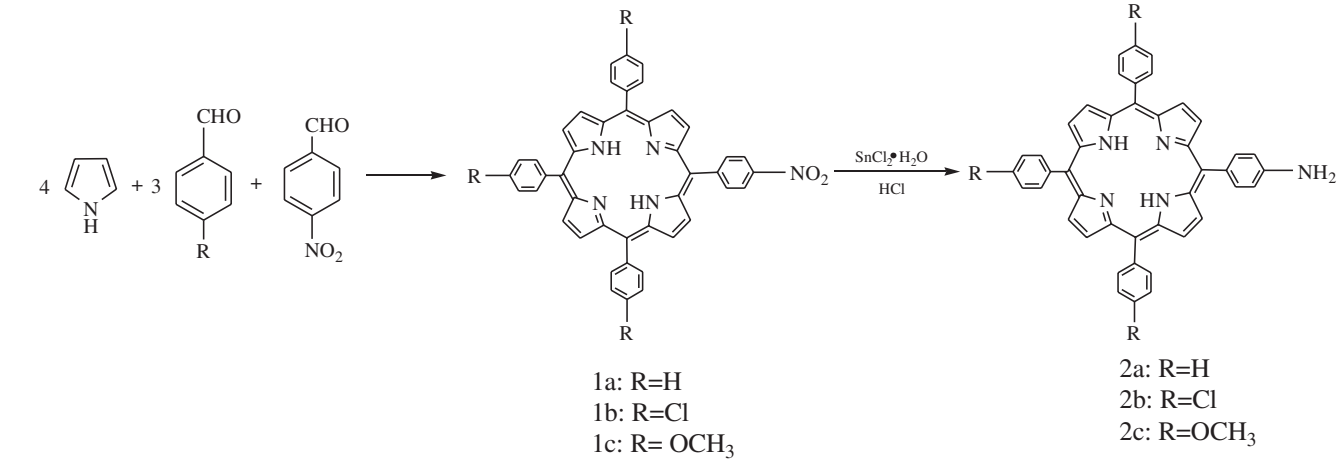

1a: R=H
1b: R=Cl
1c: R= OCH_3

2a: R=H
2b: R=Cl
2c: R=OCH_3

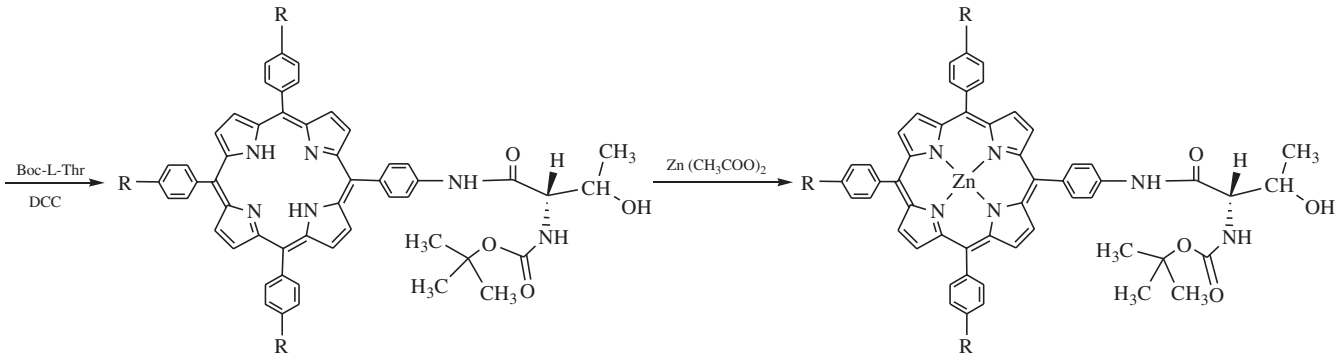

3a: R=H
3b: R=Cl
3c: R=OCH_3

4a: R=H
4b: R=Cl
4c: R=OCH_3

Scheme 1. Synthetic route of porphyrin complexes.

to react at reflux under microwave conditions for 2 min and then allowed to cool overnight. The CH_3CH_2COOH was distilled off under reduced pressure. The mixture including porphyrin **1a** was obtained as a purple powder.[28]

Porphyrin 1b: The method used was the same as that described for **1a**, but using 4-chlorobenzaldehyde.[29]

Porphyrin 1c: A mixture of 4-nitrobenzaldehyde (0.6 g, 4 m mol), *p*-methoxybenzaldehyde (1 mL, 0.051 mol), and pyrrole (0.85 mL, 8 mmol) in acetic anhydride (12 mL) was stirred and then added to glacial acetic acid (100 mL). The reaction mixture was heated under reflux for 60 min. It was then allowed to cool. After extractive work-up, the crude material was obtained as a purple powder.[30]

Porphyrin 2a: A portion of the mixture including porphyrin **1a** (30 mg) was dissolved in concentrated hydrochloric acid (80 mL). Tin(II) chloride dihydrate (2.6 g) was added, and the solution was heated at 65−70 °C for 1.5 h. It was then cooled and poured into water (100 mL), and the resulting mixture was adjusted to pH 8 with concentrated ammonium hydroxide solution. The aqueous phase was extracted with chloroform. The organic phase was concentrated to a volume of 50 mL on a rotary evaporator, and this solution was chromatographed on a silica column eluting with chloroform. The second band eluted from the column contained the desired product. Yield 18.4%. Anal. Calcd. for $C_{44}H_{31}N_5$: C, 83.94; H, 4.93; N, 11.13. Found: C, 83.61; H, 5.17; N, 11.44. ^{1}H NMR ($CDCl_3$, 400 MHz): δ = 8.83−8.95 (m, 8H, pyrrole-H), 8.20−8.23 (m, 6H, 10, 15, 20 Ar-*o*-H), 8.00 (d, 2H, 5 Ar-*o*-H), 7.75−7.77 (m, 9H, 10, 15, 20 Ar-*m*-H and *p*-H), 7.07 (d, 2H, 5 Ar-*m*-H), 4.04 (s, 2H, $ArNH_2$), −2.76 ppm (s, 2H, pyrrole NH).

Porphyrin 2b: The method used was the same as that described for **2a**. Yield 21.2%. Anal. Calcd. for $C_{44}H_{28}Cl_3N_5$: C, 72.08; H, 3.82; N, 9.56. Found: C, 71.88; H, 4.18; N, 9.14. ^{1}H NMR ($CDCl_3$, 400 MHz): δ = 8.83−8.87 (m, 8H, pyrrole-H), 8.16 (d, 6H, 10, 15, 20 Ar-*o*-H), 8.00 (d, 2H, 5 Ar-*o*-H), 7.75−7.78 (m, 6H, 10, 15, 20 Ar-*m*-H), 7.06 (d, 2H, 5 Ar-*m*-H), 4.01 (s, 2H, $ArNH_2$), −2.78 ppm (s, 2H, pyrrole NH).

Porphyrin 2c: The method used was the same as that described for **2a**. Yield 15.3%. Anal. Calcd. for $C_{47}H_{37}O_3N_5$: C, 78.44; H, 5.15; N, 9.74. Found: C, 78.01; H, 5.48; N, 9.52. ^{1}H NMR ($CDCl_3$, 400 MHz): δ = 8.85−8.99 (m, 8H, pyrrole-H), 8.13−8.16 (m, 6H, 10, 15, 20 Ar-*o*-H), 8.02 (d, 2H, 5 Ar-*o*-H), 7.28−7.32 (m, 6H, 10, 15, 20 Ar-*m*-H), 7.07 (d, 2H, 5 Ar-*m*-H), 4.09 (s, 9H, OCH_3), 4.07 (s, 2H, $ArNH_2$), −2.70 ppm (s, 2H, pyrrole NH).

Porphyrin 3a: An excess of Boc-L-threonine (20 mg, 0.11 mmol) was added to a solution of porphyrin **2a** (100 mg, 0.074 mmol) in CH_2Cl_2 (60 mL) and the mixture was stirred in an ice bath for 10 min. *N*,*N*-Dicyclohexylcarbodiimide (DCC) was added dropwise over a period of 20 min, and the mixture was stirred for a further 12 h. The ice bath was then removed, and the mixture was washed with 10% aqueous Na_2CO_3 solution and water, and dried over Na_2SO_4. After evaporation of the solvent, the resulting solid was redissolved in $CHCl_3$ and purified on a column of silica gel. A red band containing the product was collected. Yield 73.4%. Anal. Calcd. for $C_{53}H_{46}O_4N_6$: C, 76.63; H, 5.54; N, 10.12. Found: C, 76.41; H, 5.89; N, 9.82. ^{1}H NMR ($CDCl_3$, 400 MHz): δ = 8.87−8.90 (m, 8H, pyrrole H), 8.23−8.25 (m, 8H, 5, 10, 15, 20 Ar-*o*-H), 7.96 (d, 2H, 5 Ar-*m*-H), 7.78−7.79 (m, 9H, 10, 15, 20 Ar-*m*-H and *p*-H), 5.79 (d, 1H, CO-NH), 4.70 (d, 1H, α H), 4.38 (d, 1H, β H), 3.38 (s, 1H, ArNH), 1.61 (s, 9H, $C(CH_3)_3$), 1.38 (d, 3H, CH_3), −2.75 ppm (s, 2H, pyrrole NH).

Porphyrin 3b: The method used was the same as that described for **3a**. Yield 77.2%. Anal. Calcd. for $C_{53}H_{43}O_4Cl_3N_6$: C, 68.13; H, 4.61; N, 9.00. Found: C, 67.85; H, 4.30; N, 9.14. ^{1}H NMR ($CDCl_3$, 400 MHz): δ = 8.83−8.91 (m, 8H, pyrrole-H), 8.13−8.15 (m, 8H, 5, 10, 15, 20 Ar-*o*-H), 7.83−7.85 (m, 2H, 5 Ar-*m*-H), 7.75−7.78 (m, 6H, 10, 15, 20 Ar-*m*-H), 5.76 (d, 1H, CO−NH), 4.70 (s, 1H, α H), 4.37 (m, 1H, β H), 3.36 (d, 1H, ArNH), 1.60 (s, 9H, $C(CH_3)_3$), 1.39 (d, 3H, CH_3), −2.82 ppm (s, 2H, pyrrole NH).

Porphyrin 3c: The method used was the same as that described for **3a**. Yield 65.5%. Anal. Calcd. for $C_{56}H_{52}O_7N_6$: C, 73.04; H, 5.65; N, 9.13. Found: C, 73.28; H, 5.25; N, 8.74. ^{1}H NMR ($CDCl_3$, 400 MHz): δ = 8.89−8.91 (m, 8H, pyrrole-H), 8.11−8.19 (m, 8H, 5, 10, 15, 20 Ar-*o*-H), 7.93−7.95 (m, 2H, 5 Ar-*m*-H), 7.28−7.32 (m, 6H, 10, 15, 20 Ar-*m*-H), 4.68 (s, 1H, α H), 5.81 (d, 1H, CO−NH), 4.39 (m, 1H, β H), 4.11 (s, 9H, OCH_3), 3.50 (d, 1H, ArNH), 1.60 (s, 9H, $C(CH_3)_3$), 1.44 (d, 3H, CH_3), −2.74 ppm (s, 2H, pyrrole NH).

Porphyrin 4a: An excess of $Zn(OAc)_2 \cdot 2H_2O$ (20 mg, 0.11 mmol) was added to a solution of porphyrin **3a** (100 mg, 0.074 mmol) in CH_2Cl_2/MeOH (20 mL, 10:1) and the mixture was heated under reflux with exclusion of light for 1 h. Upon completion of the reaction, the solution was washed with H_2O and dried over Na_2SO_4. The mixture was filtered, the filtrate was concentrated to dryness, and the remaining material was purified on a column of silica gel ($CHCl_3$/Et_2O, 20:1, as eluent) to give the product as a red amorphous solid. Yield 89.3%. Anal. Calcd. for $C_{53}H_{44}O_4N_6Zn$: C, 71.22; H, 4.93; N, 9.41. Found: C, 71.28; H, 5.30; N, 9.14. ^{1}H NMR ($CDCl_3$, 400 MHz): δ = 8.97−8.99 (m, 8H, pyrrole H), 8.20−8.25 (m, 8H, 5, 10, 15, 20 Ar-*o*-H), 7.81−7.91 (d, 2H, 5 Ar-*m*-H), 7.54−7.79 (m, 9H, 10, 15, 20 Ar-*m*-H and *p*-H), 5.74 (d, 1H, CO−NH), 4.63 (s, 1H, α H), 4.30 (d, 1H, β H), 3.31 (s, 1H, ArNH), 1.58 (s, 9H, $C(CH_3)_3$), 1.48 ppm (d, 3H, CH_3).

Porphyrin 4b: The method used was the same as that described for **4a**. Yield 92.5%. Anal. Calcd. for $C_{53}H_{41}O_4N_6Cl_3Zn$: C, 63.82; H, 4.11; N, 8.43. Found: C, 63.97; H, 4.44; N, 8.01. ^{1}H NMR ($CDCl_3$, 400 MHz): δ = 8.94−8.97 (m, 8H, pyrrole-H), 8.15 (s, 8H, 5, 10, 15, 20 Ar-*o*-H), 7.76−7.86 (m, 8H, 5, 10, 15, 20 Ar-*m*-H), 5.63 (d, 1H, CONH), 4.44 (s, 1H, α H), 4.24 (m, 1H, β H), 3.20 (d, 1H, ArNH), 1.54 (s, 9H, $C(CH_3)_3$), 1.39 ppm (d, 3H, CH_3).

Porphyrin 4c: The method used was the same as that described for **4a**. Yield 87.4%. Anal. Calcd. for

$C_{56}H_{50}O_7N_6Zn$: C, 68.36; H, 5.09; N, 8.55. Found: C, 68.61; H, 5.54; N, 8.18. ^{1}H NMR ($CDCl_3$, 400 MHz): δ = 8.85–9.04 (m, 8H, pyrrole-H), 8.11–8.19 (m, 8H, 5, 10, 15, 20 Ar-*o*-H), 7.84–7.86 (d, 2H, 5 Ar-*m*-H), 7.28–7.32 (m, 6H, 10, 15, 20 Ar-*m*-H), 5.61 (s, 1H, CONH), 5.05 (m, 1H, α H), 4.45 (m, 1H, β H), 4.11 (s, 9H, OCH_3), 3.39 (d, 1H, ArNH), 1.49 (s, 9H, $C(CH_3)_3$), 1.30 ppm (d, 3H, CH_3).

Results and Discussion

UV/vis Spectra. Figures 1 and 2 show the UV/vis spectra of the free base porphyrins and zinc porphyrins in CH_2Cl_2, and the data are listed in Table 1. Salient features can be summarized as follows: (1) In Figure 1, traces A and a, B and b, and C and c show the UV/vis spectra of porphyrins **3a**, **3b**, and **3c**, respectively. The three kinds of free-base porphyrins each showed four Q bands and one Soret band. The Soret band was at ~420 nm, and the Q bands were in the region 500 –700 nm. (2) In Figure 2, traces A and a, B and b, and C and c are the UV/vis spectra of porphyrins **4a**, **4b**, and **4c**, respectively. The three kinds of zinc porphyrins each showed two Q bands and one Soret band. Compared to those of the corresponding free porphyrins, the Soret band and the Q bands of the zinc porphyrins were somewhat shifted. (3) As shown in Table 1, the value of molar extinction coefficient ε for **3a** is exceptionally large (~8×10^5 L/(M/cm)) compared to other free porphyrins. Also, the value of ε in Soret band for **3a** is larger (about twofold) than that of **3b** and **3c**, but the Q band is smaller than that of **3c**. For three zinc porphyrins, the value of ε in Soret band for **4a** is the highest, and the value of ε in Q band for **4c** is the smallest.

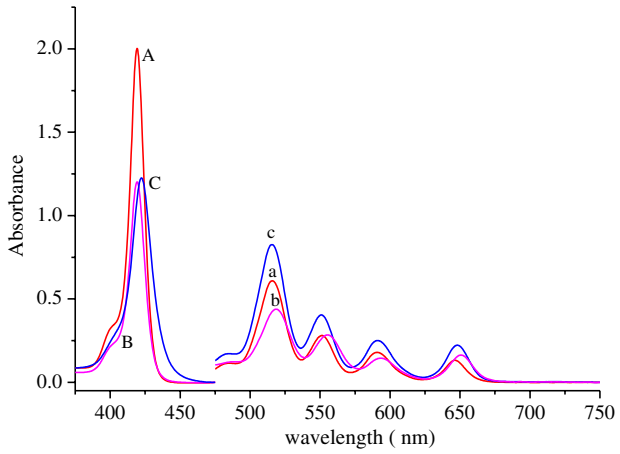

Figure 1. UV–vis spectra of free base porphyrins. Soret band: **3a** (trace A); **3b** (trace B); **3c** (trace C). Q band: **3a** (trace a); **3b** (trace b); **3c** (trace c).

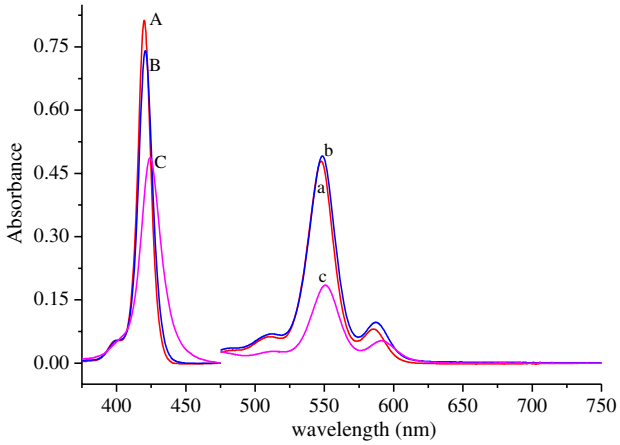

Figure 2. UV–vis spectra of zinc porphyrins. Soret band: **4a** (trace A); **4b**(trace B); **4c**(trace C). Q band: **4a** (trace a); **4b** (trace b); **4c** (trace c).

It has been shown that the classic Goutermans four-orbital model can explain the absorption properties of porphyrins.[31] The UV/vis absorption bands of porphyrins are due to the electronic transitions from the ground state (S_0) to the two lowest singlet excited states S_1 and S_2. The $S_0 \rightarrow S_1$ transition gives rise to the weak Q bands in visible region, whereas the $S_0 \rightarrow S_2$ transition produces the strong Soret band in the near-UV region. After metal ion incorporation into the porphyrin, the number of Q bands decreases, and the absorption frequencies are shifted due to the change in molecular symmetry.

^{1}H NMR Spectra. ^{1}H NMR spectra of porphyrins **2a–2c**, **3a –3c**, and **4a–4c** were measured in $CDCl_3$ solution. The data are listed in the synthesis section. Salient features can be summarized as follows: (1) The ^{1}H chemical shifts of NH_2 in porphyrins **2a**, **2b**, and **2c** are δ = 4.04, 4.01, and 4.07 ppm. In porphyrins **3a**, **3b**, and **3c**, due to the impact of the amino acid, the ^{1}H chemical shifts are δ = 3.38, 3.36, and 3.50 ppm, and the amide protons of the Boc-amino acid give rise to signals at δ = 5.79, 5.76, and 5.81 ppm. This confirmed the reaction between the Boc-amino acid and porphyrins **2a**, **2b**, and **2c** to afford free porphyrin compounds. (2) The ^{1}H chemical shifts of the two protons inside the porphyrin ring in **3a**, **3b**, and **3c** are −2.75, −2.82, and −2.74 ppm, respectively. In porphyrins **4a**, **4b**, and **4c**, these resonances are no longer seen, confirming the formation of the zinc porphyrin complexes.

Isosbestic Point Diagram. Titrations of porphyrin **4a** with Im and *N*-MeIm were studied by UV/vis spectrophotometry. Inspection of Figure 3(a) reveals that, upon the addition of Im to a solution of porphyrin **4a**, the absorption intensity of **4a** gradually diminished, while that of the product gradually increased. The original Soret band of porphyrin **4a** was red-shifted from 419.8 to 429.5 nm. A clear isosbestic point in the UV/vis spectra of the porphyrin **4a**–Im system was observed at 425.2 nm. Similar spectral changes were observed for the porphyrin **4a**–*N*-MeIm (Figure 3(b)), **4b**–Im and **4b**–*N*-MeIm, as well as **4c**–Im and **4c**–*N*-MeIm systems.

The observed spectral changes, involving the consumption of porphyrin **4a** and the formation of isosbestic points, are characteristic of axial coordination to a zinc porphyrin, confirming that the zinc porphyrins reacted with Im and *N*-MeIm. Im and *N*-MeIm are strongly nucleophilic small molecules. When coordinating to zinc porphyrins, they changed the electron density in the porphyrin ring.[32–34] The position of

Table 1. Data of UV–vis spectra.

Porphyrins	Soret band, nm ($\varepsilon \times 10^{-5}$ L/(M/cm))	Q band, nm ($\varepsilon \times 10^{-4}$ L/(M/cm))			
		Q_I	Q_{II}	Q_{III}	Q_{IV}
3a	419.2(8.01)	515.8(2.46)	551.4(1.14)	590.8(0.74)	646.4(0.91)
3b	419.2(4.83)	516.0(1.78)	551.2(1.17)	591.7(0.59)	648.6(0.66)
3c	424.2(4.92)	518.6(3.30)	555.2(1.63)	593.8(1.02)	651.2(0.91)
4a	419.8(3.25)		547.8(1.93)	585.4(0.33)	
4b	420.2(2.96)		548.6(1.98)	586.9(0.40)	
4c	425.9(1.96)		560.1(0.74)	596.0(0.22)	

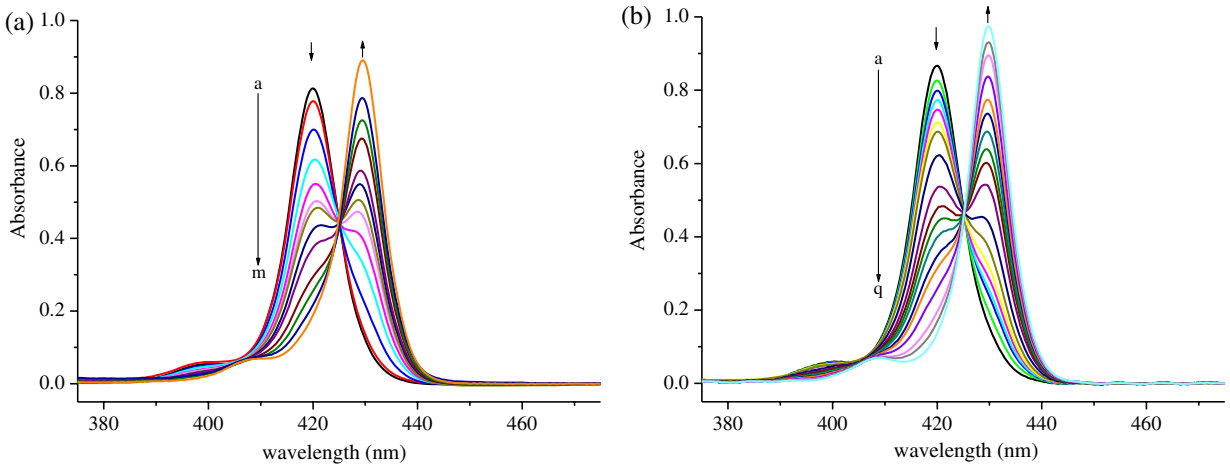

Figure 3. The isosbestic points of systems. (A) **4a**–Im system at 5 °C (a: **4a**, 2.5 μM; b–m: $c_{Im}/c_{\mathbf{4a}} = 0.2, 1, 2, 3, 4, 5, 6, 8, 15, 20, 40, 50$). (B) **4a**–*N*-MeIm system at 10 °C (a: **4a**, 2.5 μM; b-q: $c_{N\text{-MeIm}}/c_{\mathbf{4a}} = 0.4, 0.6, 0.8, 1, 1.4, 1.6, 2, 3, 4, 5, 6, 8, 10, 15, 30, 50, 300$).

the maximum absorption peak in the axial coordination system is not changed with increasing concentration of Im or *N*-MeIm, illustrating that the coordination number of the system remains unchanged.

The Value *n* and Association Constant K^{θ}. The value *n* and association constant K^{θ} of a coordination system are given by the equation[35,36] $\ln[(A_0 - A_e)/(A_e - A_\infty)] = n \ln c_L + \ln K^{\theta}$. In the present system, A_0 is the absorbance of the zinc porphyrin solution, A_e is the equilibrium absorbance of zinc porphyrin–imidazole system, and A_∞ is the equilibrium absorbance of the zinc porphyrin–imidazole system after complete conversion of the reactants to the complex. Here, *n* is a constant indicating the ratio of imidazole derivative to zinc porphyrin in the system, and K^{θ} is the association constant [$K^{\theta} = K$/(mol/L)].

The values of *n* and the association constants K^{θ} for the coordination systems are summarized in Tables 2 and 3, respectively. Plots of $\ln[(A_0-A_e)/(A_e-A_\infty)]$ vs. $\ln c_L$ constructed from the experimental results showed good linear correlations ($r > 0.995$). As shown in Table 2, the values of *n* were all close to 1 at various temperatures, indicating the formation of 1:1 complexes between porphyrins **4a**, **4b**, and **4c** and Im or *N*-MeIm. Zn(II) has a d^{10} electron configuration, and according to ligand field theory generally prefers to reside in a tetrahedral field. When a number of ligands or ions interact with the zinc porphyrin, the zinc ion is slightly displaced from the plane of the porphyrin, and its increased electronegativity allows the binding of a fifth ligand. That is to say, besides the four N atoms of the porphyrin ring, the Zn^{2+} is also coordinated by an imidazole derivative, resulting in a five-coordinate system.

Table 2. Value *n* of the coordination reaction.

Porphyrins	Imidazole derivatives	*n*				
		5 °C	10 °C	15 °C	20 °C	$n_{average}$
4a	Im	1.04	1.03	1.02	1.03	1.03
	N-MeIm	1.12	1.11	1.09	1.08	1.10
4b	Im	1.09	1.08	1.09	1.06	1.08
	N-MeIm	1.09	1.07	1.07	1.06	1.08
4c	Im	1.00	0.99	0.96	0.97	0.98
	N-MeIm	0.99	0.99	0.99	1.00	0.99

From Table 3, we can state the following: (1) For the same porphyrin and the same imidazole derivative, the association constants K^{θ} decreased with increasing temperature, illustrating that the coordination reaction was spontaneous. (2) For the same porphyrin and different imidazole derivatives, the association constants for axial coordination decreased in the order K(*N*-MeIm) > K(Im). The superior coordinating ability of *N*-MeIm can be attributed to increased electron density on the coordinating nitrogen atom due to the electron-donating

meta-methyl substituent. (3) For the different porphyrins with the same imidazole derivative, the system porphyrin **4b**–*N*-MeIm showed the highest association constant. This is because the electron-withdrawing chloro substituents in **4b** increased the electropositivity of the zinc ion in the porphyrin plane, thereby enhancing the coordination ability. Conversely, the electron-donating methoxy group in **4c** decreased the electropositivity of the zinc ion in the porphyrin plane, thereby weakening the coordination ability of **4c**.

Thermodynamic Parameters. In order to gain further insight into the interaction mechanism, we determined the thermodynamic parameters for the present coordination reactions according to the van't Hoff equation[37,38] $\ln K^{\theta} = -\Delta_r H_m^{\theta}/RT + \Delta_r S_m^{\theta}/R$, where R is the universal gas constant and T is the temperature in degrees kelvin. Accordingly, the enthalpy and entropy changes associated with these reactions were obtained from the slope and intercept, respectively, of linear plots of $\ln K^{\theta}$ versus T^{-1}. The Gibbs free energies $\Delta_r G_m^{\theta}$ were calculated according to the equation $\Delta_r G_m^{\theta} = \Delta_r H_m^{\theta} - T\Delta_r S_m^{\theta}$. The values of $\Delta_r G_m^{\theta}$, $\Delta_r H_m^{\theta}$, and $\Delta_r S_m^{\theta}$ are listed in Table 4. From Table 4, the following conclusions can be drawn: (1) The $\Delta_r G_m^{\theta}$ values showed that the complex formation was spontaneous. (2) The magnitude of $-\Delta_r H_m^{\theta}$ was larger than that of $-\Delta_r S_m^{\theta}$ for each system, indicating that the enthalpy change was the main driving force of the coordination process. (3) The value of $\Delta_r S_m^{\theta}$ for each system was negative, indicating a decrease in the degree of freedom of the components upon complexation, which could be ascribed to the restriction of translational, rotational, and internal rotational motions upon binding.[39] (4) The most negative values of $\Delta_r G_m^{\theta}$ and $\Delta_r H_m^{\theta}$ for the **4b**–*N*-MeIm system indicated the strongest interactions.

Theoretical Calculations. The properties of these molecules mainly depend on their geometrical structures. Consequently, it was very important to determine the structures of the systems. The optimized geometries of systems **4a**–Im and **4a**–*N*-MeIm are given in Figure 4. Table 5 lists the total energies, the Mulliken charges on the Zn atoms, the Zn–N bond lengths, and bond energies for each of the systems.

We consider first **4a**, **4b**, and **4c**. Compared to the charge on Zn^{2+} in the structure of **4a** (1.071 *e*), the charge on Zn^{2+} in **4b** was larger (1.074 *e*), whereas that on the Zn^{2+} in **4c** was smaller (1.068 *e*). The results indicated that the Cl substituents increased the charge on Zn^{2+}, whereas the methoxy substituents decreased the charge on Zn^{2+}.

When Im was bound to the zinc porphyrins (**4a**, **4b**, and **4c**), the charges on Zn^{2+} were reduced to 1.041, 1.042, and 1.039 *e*, respectively. The bond lengths for **4a**–Im, **4b**–Im, and **4c**–Im were determined as 2.242, 2.238, and 2.244 Å, respectively, and the corresponding bond energies were 62.2, 65.3, and 61.1 kJ/mol. The results indicated that the Cl substituents increased the bond energy, such that the zinc porphyrin–Im complex was more tightly bound. However, the methoxy

Table 3. Association constants K^{θ} of the coordination reaction.

Porphyrins	Imidazole derivatives	K^{θ} 5 °C	10 °C	15 °C	20 °C
4a	Im	$(1.26 \pm 0.03) \times 10^5$ $r = 0.9992$	$(9.21 \pm 0.02) \times 10^4$ $r = 0.9988$	$(6.68 \pm 0.01) \times 10^4$ $r = 0.9995$	$(4.74 \pm 0.04) \times 10^4$ $r = 0.9989$
	N-MeIm	$(5.46 \pm 0.01) \times 10^5$ $r = 0.9991$	$(3.43 \pm 0.03) \times 10^5$ $r = 0.9989$	$(2.28 \pm 0.03) \times 10^5$ $r = 0.9993$	$(1.59 \pm 0.02) \times 10^5$ $r = 0.9996$
4b	Im	$(2.43 \pm 0.02) \times 10^5$ $r = 0.9989$	$(1.64 \pm 0.04) \times 10^5$ $r = 0.9995$	$(1.12 \pm 0.04) \times 10^5$ $r = 0.9991$	$(7.62 \pm 0.03) \times 10^4$ $r = 0.9991$
	N-MeIm	$(1.01 \pm 0.01) \times 10^6$ $r = 0.9997$	$(6.38 \pm 0.02) \times 10^5$ $r = 0.9992$	$(3.65 \pm 0.04) \times 10^5$ $r = 0.9998$	$(2.37 \pm 0.04) \times 10^5$ $r = 0.9998$
4c	Im	$(1.04 \pm 0.03) \times 10^5$ $r = 0.9988$	$(7.92 \pm 0.01) \times 10^4$ $r = 0.9992$	$(6.15 \pm 0.04) \times 10^4$ $r = 0.9993$	$(4.59 \pm 0.01) \times 10^4$ $r = 0.9992$
	N-MeIm	$(2.22 \pm 0.04) \times 10^5$ $r = 0.9990$	$(1.67 \pm 0.03) \times 10^5$ $r = 0.9992$	$(1.23 \pm 0.03) \times 10^5$ $r = 0.9992$	$(9.30 \pm 0.04) \times 10^4$ $r = 0.9990$

r is the linear correlation coefficient.

Table 4. Thermodynamic data of the coordination reactions.

Porphyrins	Imidazole derivatives	$\Delta_r H_m^{\theta}$ (kJ/mol)	$\Delta_r S_m^{\theta}$ (J/(mol/K)	$\Delta_r G_m^{\theta}$ (kJ/mol)	*r*
4a	Im	−44.12	−60.86	−25.97	0.9993
	N-MeIm	−55.72	−90.62	−28.70	0.9991
4b	Im	−50.73	−79.32	−27.08	0.9995
	N-MeIm	−66.43	−123.80	−29.52	0.9990
4c	Im	−36.82	−36.25	−26.01	0.9993
	N-MeIm	−39.56	−39.82	−27.69	0.9999

r is the linear correlation coefficient.

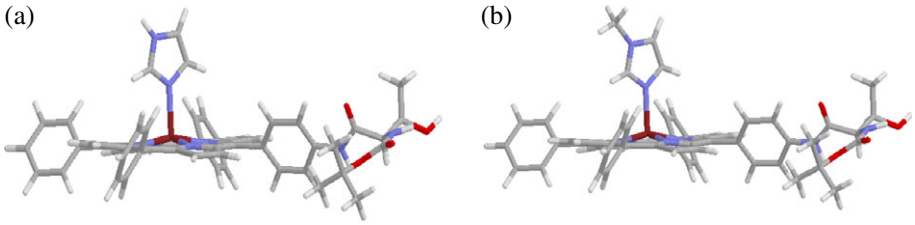

Figure 4. The structures of system-optimized geometries. (a) **4a**–Im and (b) **4a**–*N*-MeIm).

Table 5. Quantum chemistry results of system.

Porphyrins	Charge$_{Zn}$ (e)	Combination energy (kJ/mol)	Bond length (Å) (Zn–N)
4a	1.071		
4b	1.074		
4c	1.068		
4a-Im	1.041	62.2	2.242
4b-Im	1.042	65.3	2.238
4c–Im	1.039	61.1	2.244
4a–*N*-MeIm	1.040	64.2	2.235
4b–*N*-MeIm	1.041	67.6	2.231
4c–*N*-MeIm	1.038	63.0	2.237

substituents decreased the bond energy, leading to a less tightly bound complex, in agreement with the experimental results.

The combination energies for **4a**–*N*-MeIm (64.2 kJ/mol), **4b**–*N*-MeIm (67.6 kJ/mol), and **4c**–*N*-MeIm (63.0 kJ/mol) were calculated to be larger than those for **4a**–Im, **4b**-Im and **4c**–Im by ~2.0 kJ/mol. The Zn–N bond lengths for **4a**–*N*-MeIm (2.235 Å), **4b**–*N*-MeIm (2.231 Å), and **4c**–*N*-MeIm (2.237 Å) were calculated to be shorter than those for **4a**–Im, **4b**–Im, and **4c**–Im by about 0.07 Å. The results supported the conclusion that the bonding between the zinc porphyrins and *N*-MeIm was stronger than that between the zinc porphyrins and Im.

Fluorescence Spectra. The coordination reactions between zinc porphyrins and imidazole derivatives were also studied on the basis of fluorescence measurements at room temperature. Upon excitation of the Soret band of zinc porphyrins at 420 nm, the fluorescence emission spectra in CH_2Cl_2 are shown in Figures 5–7.[40]

There appears fluorescence of the S_2 (Soret band) and the S_1 (Q bands) in the porphyrin complexes. The fluorescence of Soret band is attributed to the transition from the second excited state S_2 to the ground state S_0, which is much weaker than for the $S_1 \rightarrow S_0$ transition of the Q band emission. And then, the S_1 state, whose fluorescence lifetime is the nanosecond scale, is in a dominant position in the photochemical reaction of porphyrin molecules.[41–43] For **4a**, **4b**, and **4c**, the fluorescence of S_1 consisted of two bands. From inspection of Figures 5–7, the following conclusions can be drawn:

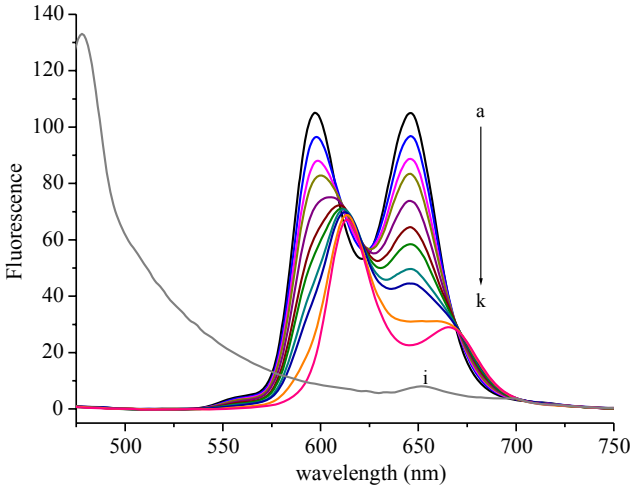

Figure 5. Fluorescence spectra of the system **4a**–*N*-MeIm. (**a**: **4a**, 2.5 μM; b–k: $c_{\textbf{N-MeIm}}/_{\textbf{4a}} = 2, 4, 6, 10, 15, 20, 30, 40, 100, 300$; i: *N*-MeIm, 7.50×10^{-4} M).

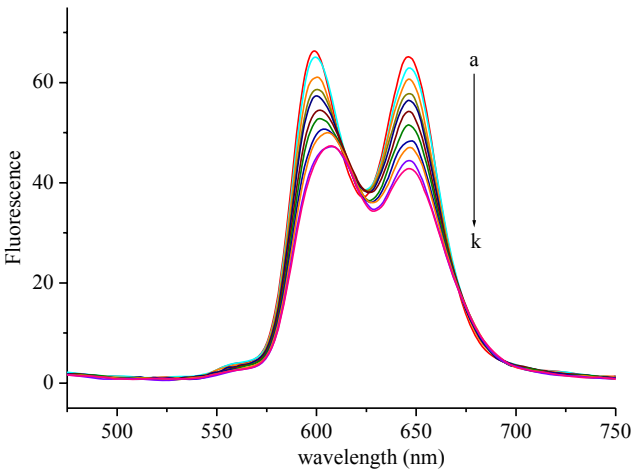

Figure 6. Fluorescence spectra of the system **4b**–*N*-MeIm. (**a**: **4b**, 2.5 μM; b–k: $c_{\textbf{N-MeIm}}/c_{\textbf{4b}} = 1.5, 2.4, 3, 3.4, 5, 5.4, 7, 8, 8.4, 10$).

1. The characteristic peaks of the S_1 states of **4a**, **4b**, and **4c** are 597.0 and 644.8 nm, 599.1 and 645.9 nm, 603.2 and 649.8 nm, respectively. Compared to those of **4a**, the emission peaks of **4b** and **4c** show bathochromic shift. This indicates that the porphyrin macrocycle conjugation is affected by Cl and methoxy substituents.
2. The characteristic fluorescence peak of *N*-MeIm is at 652.7 nm (line i in Figure **5**) and the fluorescence intensity is very low. When different concentrations of *N*-

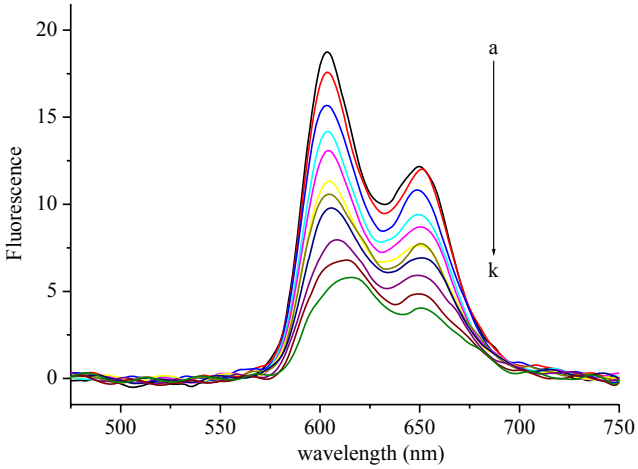

Figure 7. Fluorescence spectra of the system **4c**–*N*-MeIm. (a: **4c**, 2.5 μM; b–k: $c_{N\text{-MeIm}}/c_{4c} = 0.8, 2, 3, 5, 6, 7, 10, 15, 20, 30$).

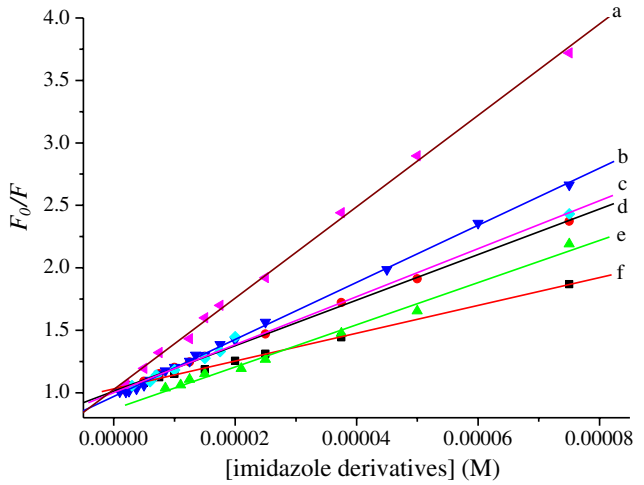

Figure 8. The Stern–Volmer curves. (a: **4c**–*N*-MeIm; b: **4b**–*N*-MeIm; c: **4c**–Im; d: **4a**–*N*-MeIm; e: **4b**–Im; f: **4a**–Im).

MeIm were added to a solution of zinc porphyrin of a certain concentration, the fluorescence spectrum of the mixed system changed considerably, which was not a simple superposition of the spectra of the zinc porphyrin and *N*-MeIm. This indicated that the configuration of the complex was changed after the coordination of *N*-MeIm, with the symmetry of the molecule changing from the original D_{4h} to C_{4v}. The luminescent properties of the zinc porphyrin were thus changed, as borne out by the UV spectroscopic results.

3. With increasing concentration of *N*-MeIm, the emission intensity of **4a**, **4b**, and **4c** decreased, which may be due to efficient photoinduced electron transfer between zinc porphyrin and *N*-MeIm. When $c_{N\text{-MeIm}}/c_{4a}$, $c_{N\text{-MeIm}}/c_{4b}$, $c_{N\text{-MeIm}}/c_{4c}$ is 300, 10, 30, respectively, the intensity of the spectra was almost unchanged, indicating that fluorescence quenching was induced by the complex.[42,44] This was clearly the consequence of the interaction between zinc porphyrin and imidazole derivative. The imidazole N atom bore lone pair electrons before the coordination reaction. On one hand, this N atom formed a σ-bond with Zn^{2+} upon coordination, while, on the other, the Zn^{2+} ion engaged in π-backbonding with the N atom through its d electrons, the π-backbonding changed the electron density of the porphyrin ring, and the distribution of the electron cloud was more uneven over the whole conjugation system. The symmetry of the molecule was thereby reduced, which changed the vibrational mode of the S_1 state. Thus, nonradiative transition from S_1 to T_1 was strengthened, and the fluorescence intensity of the complex decreased. That is to say, fluorescence quenching occurred between the zinc porphyrins and the imidazole derivatives. Similar changes in the fluorescence spectra were observed for the various zinc porphyrins with Im.
4. In order to qualitatively explore the quenching mechanism, we obtained the Stern–Volmer quenching constant K_{sv} and the quenching rate constant K_q according to the equation $F_0/F = 1 + K_q\tau_0[Q] = 1 + K_{sv}[Q]$.[45] A linear relationship was obtained by plotting and fitting F_0/F against $[Q]$, as shown in Figure 8. The values are listed in Table 6. The plots revealed a certain degree of slope, indicating the occurrence of efficient quenching between the zinc porphyrin and imidazole derivatives.

Table 6. Quenching rate constant K_q at room temperature.

Systems	$F_0/F - [Q]$	K_q (L/(mol/s))	r
4a–*N*-MeIm	1.0101 + 18 414[*Q*]	(1.84 ± 0.001)×10^{12}	0.9992
4a–Im	1.0311 + 11 094[*Q*]	(1.11 ± 0.001)×10^{12}	0.9997
4b–*N*-MeIm	0.9701 + 22 836[*Q*]	(2.28 ± 0.004)×10^{12}	0.9994
4b–Im	0.9729 + 16 676[*Q*]	(1.67 ± 0.003)×10^{12}	0.9991
4c–*N*-MeIm	1.0265 + 36 555[*Q*]	(3.66 ± 0.005)×10^{12}	0.9990
4c–Im	1.0045 + 18 920[*Q*]	(1.89 + 0.002) ×10^{12}	0.9992

r is the linear correlation coefficient.

As shown in Table 6, the values of the quenching rate constants K_q between the various zinc porphyrins and imidazole derivatives were all much larger than 2.0×10^{10} L/(mol/s) (the constant of maximum diffusion collision quenching rate), which was caused by formation of the complex before excitation occurred. The **4c**–*N*-MeIm system showed the highest quenching rate constant K_q. In other words, the chemical reaction between zinc porphyrins and imidazole derivatives at different concentrations led to a quenching effect.

Conclusion

Porphyrins and threonine have important biological functions. In order to combine their biological activities, we have synthesized three kinds of free porphyrins modified with

Boc-L-threonine as well as their zincated analogs. We studied the interaction between these zinc porphyrins and imidazole derivatives by means of UV/vis spectroscopy, fluorescence spectroscopy, and quantum chemical methods. The results showed the following: (1) The reaction was spontaneous, with a coordinative bond being formed between the zinc porphyrins and imidazole derivatives. The values of n, the association constants K^{θ}, and the thermodynamic parameters $\Delta_r G_m^{\theta}$, $\Delta_r H_m^{\theta}$, and $\Delta_r S_m^{\theta}$ of the coordination reaction were determined at four different temperatures. The enthalpy change was identified as the main driving force of the coordination process. (2) The binding strengths of the complexes are related to the electron-withdrawing or electron-donating nature of substituent groups on the zinc porphyrins and the structures of the imidazole derivatives. (3) Bond lengths, charges, and bond energies for the coordination reaction determined by quantum chemical calculations were consistent with the experimental results. (4) Fluorescence quenching was observed between the various zinc porphyrins and imidazole derivatives.

Acknowledgments. This work was supported by the Natural Science Foundation of Hebei Province under Grant B2014408009; the Key Project of Colleges and Universities in Hebei Province Science and Technology Research under Grant ZD20131050; the Key Program Fund of Langfang Teachers University under Grant LSZZ201301; and the Undergraduate Training Programs for Innovation and Entrepreneurship in Hebei Province under Grant 201410100007.

References

1. J. X. Jiang, Z. Q. Feng, B. Z. Liu, C. J. Hu, Y. Wang, *Dalton Trans.* **2013**, *42*, 7651.
2. S. Ishihara, J. Labuta, W. V. Rossom, D. Ishikawa, K. Minami, J. P. Hillab, K. Ariga, *Phys. Chem. Chem. Phys.* **2014**, *16*, 9713.
3. V. K. Praveen, C. Ranjith, E. Bandini, A. Ajayaghosh, N. Armaroli, *Chem. Soc. Rev.* **2014**, *43*, 4222.
4. M. Raynal, P. Ballester, A. Vidal-Ferran, P. W. N. M. Leeuwen, *Chem. Soc. Rev.* **2014**, *43*, 1734.
5. J. K. Choi, G. Sargsyan, B. D. Johnson, M. Balaz, *RSC Adv.* **2015**, *5*, 15916.
6. S. Brahma, S. A. Ikbal, S. P. Rath, *Inorg. Chem.* **2014**, *53*, 49.
7. S. Brahma, S. A. Ikbal, A. Dhamija, S. P. Rath, *Inorg. Chem.* **2014**, *53*, 2381.
8. M. Anyika, H. Gholami, K. D. Ashtekar, R. Acho, B. Borhan, *J. Am. Chem. Soc.* **2014**, *136*, 550.
9. L. G. Yang, Y. Zhou, M. L. Zhu, L. Y. Zhao, L. Y. Wei, Y. Z. Bian, *J. Org. Chem.* **2013**, *78*, 9949.
10. T. Benelli, L. Angiolini, D. Caretti, M. Lanzi, L. Mazzocchetti, E. Salatelli, L. Giorgini, *Dyes Pigm.* **2014**, *106*, 143.
11. S. Brahma, S. A. Ikbal, S. Dey, S. P. Rath, *Chem. Commun.* **2012**, *48*, 4070.
12. N. Marets, V. Bulach, M. W. Hosseini, *New J. Chem.* **2013**, *37*, 3549.
13. O. Oviedo, T. Zoltan, F. Vargas, M. Inojosa, J. Vivas, *J. Coord. Chem.* **2014**, *67*, 1715.
14. D. Quezada, J. Honores, M. J. Aguirre, M. Isaacs, *J. Coord. Chem.* **2014**, *67*, 4090.
15. L. Angiolini, T. Benelli, L. Giorgini, *React. Funct. Polym.* **2011**, *71*, 204.
16. S. G. Chen, Y. Yu, X. Zhao, Y. G. Ma, X. K. Jiang, Z. T. Li, *J. Am. Chem. Soc.* **2011**, *133*, 11124.
17. T. Hirose, F. Helmich, E. W. Meijer, *Angew. Chem. Int. Ed.* **2013**, *52*, 304.
18. J. X. Jiang, X. S. Fang, B. Z. Liu, C. J. Hu, *Inorg. Chem.* **2014**, *53*, 3298.
19. B. Z. Liu, J. X. Jiang, X. S. Fang, C. Hu, *Chin. J. Chem.* **2014**, *32*, 797.
20. I. C. Pintre, S. Pierrefixe, A. Hamilton, V. Valderrey, C. Bo, P. Ballester, *Inorg. Chem.* **2012**, *51*, 4620.
21. K. Yoosaf, J. Iehl, I. Nierengarten, M. Hmadeh, A. M. A. Gary, J. F. Nierengarten, N. Armaroli, *Chem. Eur. J.* **2014**, *20*, 223.
22. M. E. El-Khouly, S. Fukuzumi, F. D'Souza, *ChemPhysChem* **2014**, *15*, 30.
23. V. J. Venditto, D. S. Watson, M. Motion, D. Montefiori, F. C. Szoka, J. Rational, *Clin. Vaccine Immunol.* **2013**, *20*, 39.
24. N. Darbinian, K. Khalili, S. Amimi, *J. Cell. Physiol.* **2014**, *229*, 153.
25. A. D. Becke, *J. Chem. Phys.* **1993**, *98*, 5648.
26. C. Lee, W. T. Yang, R. G. Parr, *Phys. Rev. B.* **1988**, *37*, 785.
27. M. J. Frisch, G. W. Trucks, H. B. Schlegel, G. E. Scuseria, M. A. Robb, J. R. Cheeseman, G. Scalmani, V. Barone, B. Mennucci, G. A. Petersson, H. Nakatsuji, M. Caricato, X. Li, H. P. Hratchian, A. F. Izmaylov, J. Bloino, G. Zheng, J. L. Sonnenberg, M. Hada, M. Ehara, K. Toyota, R. Fukuda, J. Hasegawa, M. Ishida, T. Nakajima, Y. Honda, O. Kitao, H. Nakai, T. Vreven, J. A. Montgomery Jr.. , J. E. Peralta, F. Ogliaro, M. Bearpark, J. J. Heyd, E. Brothers, K. N. Kudin, V. N. Staroverov, R. Kobayashi, J. Normand, K. Raghavachari, A. Rendell, J. C. Burant, S. S. Iyengar, J. Tomasi, M. Cossi, N. Rega, J. M. Millam, M. Klene, J. E. Knox, J. B. Cross, V. Bakken, C. Adamo, J. Jaramillo, R. Gomperts, R. E. Stratmann, O. Yazyev, A. J. Austin, R. Cammi, C. Pomelli, J. W. Ochterski, R. L. Martin, K. Morokuma, V. G. Zakrzewski, G. A. Voth, P. Salvador, J. J. Dannenberg, S. Dapprich, A. D. Daniels, Ö. Farkas, J. B. Foresman, J. V. Ortiz, J. Cioslowski, D. J. Fox, *Gaussian 09, Revision A.1*, Gaussian, Inc., Wallingford, CT, **2009**.
28. S. J. Wang, W. J. Ruan, D. B. Luo, Z. A. Zhu, *Acta Chim. Sinica.* **2004**, *62*, 2165.
29. Y. B. She, K. Li, C. M. Wang, W. Wang, Z. L. Zhang. China patent. CN: 103214492 A. 2013.07.24.
30. M. Pizzotti, R. Ugo, E. Annoni, S. Quici, I. L. Rak, G. Zerbi, M. D. Zoppo, P. Fantucci, I. Invernizzi, *Inorg. Chim. Acta* **2002**, *340*, 70.
31. M. J. Gouterman, *Chem. Phys.* **1959**, *30*, 1139.
32. K. Harada, M. Fujitsuka, A. Sugimoto, T. Majima, *J. Phys. Chem. C* **2007**, *111*, 11430.
33. M. U. Winters, J. Kärnbratt, M. Eng, C. J. Wilson, H. L. Anderson, B. Albinsson, *Phys. Chem. C.* **2007**, *111*, 7192.
34. X. Y. Li, M. Tanasova, C. Vasileiou, B. Borhan, *J. Am. Chem. Soc.* **2008**, *130*, 1885.
35. W. J. Ruan, Z. A. Zhu, H. W. Chen, Z. H. Zhang, Y. Shao, R. T. Chen, *Chem. J. Chin. Univ.* **1998**, *19*, 184.
36. J. R. Miller, C. D. Dorough, *J. Am. Chem. Soc.* **1952**, *74*, 3977.

37. S. J. Wang, N. Zang, W. J. Ruan, Z. A. Zhu, *Acta. Phys. Chim. Sin.* **2008**, *24*, 507.
38. H. Dehghani, M. R. Mansournia, *Spectrochim. Acta, Part A* **2009**, *74*, 324.
39. T. Mizutani, K. Wada, S. Kitagawa, *J. Org. Chem.* **2000**, *65*, 6097.
40. E. Maligaspe, F. D'Souza, *Org. Lett.* **2010**, *12*, 624.
41. J. Aaviksoo, A. Freiberg, S. Savikhin, *Chem. Phys. Lett.* **1984**, *111*, 275.
42. J. Feng, H. J. Zhang, J. F. Xiang, X. C. Ai, X. K. Zhang, G. Z. Xu, J. P. Zhang, *Sci. China (Ser. B)* **2003**, *33*, 8.
43. E. J. Sun, Y. H. Shi, P. Zhang, M. Zhou, Y. H. Zhang, X. X. Tang, T. S. Shi, *J. Mol. Struct.* **2008**, *889*, 28.
44. S. Yagi, M. Ezone, I. Yonekura, T. Takagishi, H. Nakazumi, *J. Am. Chem. Soc.* **2003**, *125*, 4068.
45. F. D'Souza, M. E. E. Khouly, S. Gadde, A. L. Mccarty, P. A. Karr, M. E. Zandler, Y. Araki, O. Ito, *J. Phys. Chem. B* **2005**, *109*, 10107.

